INTERNATIONAL JOURNAL OF CLIMATOLOGY
Int. J. Climatol. **33**: 1015–1020 (2013)
Published online 30 March 2012 in Wiley Online Library
(wileyonlinelibrary.com) DOI: 10.1002/joc.3488

An orchestrated climate song from the Pacific and Atlantic Oceans and its implication on climatological processes

T. Lee,[a]* T. B. M. J. Ouarda[b] and J. Li[c]

[a] *Department of Civil Engineering, ERI, Gyeongsang National University, 501 Jinju-daero, Jinju, Gyeongsangnam-do 660-701, South Korea*
[b] *Department of Water and Environmental Engineering, Masdar Institute of Science and Technology, P.O. Box 54224, Abu Dhabi, UAE*
[c] *State Key Laboratory of Numerical Modeling for Atmospheric Sciences and Geophysical Fluid Dynamics (LASG), P.O. Box 9804, Beijing 100029, China*

ABSTRACT: A climate index is a time series that quantifies the temporal evolution of a climate process in a particular region. Various climatic patterns, such as the El Niño-Southern Oscillation, Pacific Decadal Oscillation (PDO), Arctic Oscillation, and North Atlantic Oscillation (NAO), have been summarized into climate indices corresponding to the respective regions; a comparison among these indices enables various further inferences. In this study, we investigated the interconnection between the Pacific and Atlantic Oceans using the representative climate indices, i.e. the PDO and NAO indices, respectively. Using empirical mode decomposition (EMD) and statistical analysis, it was shown that these two indices share the same long-term oscillation phase in the low-frequency domain, while in the high-frequency domain, the cross-correlation and the serial correlations of the two indices vary according to the phase of the long-term oscillation. This implies that a certain long-term oscillatory forcing influences both the Atlantic and Pacific regions. Three global gridded climate variables [i.e. sea-level pressure (SLP), precipitable water (PW), and sea-surface temperature (SST)] were studied over three different periods (i.e. the negative phase period of the long-term oscillation centered on 1960 and the positive phase centered on 1990). The mean 11 year anomalies revealed a noticeable particular spatial pattern and opposing tendencies for these periods. Furthermore, the global spatial patterns inducing the cross-correlation between the NAO and PDO indices and the lag-1 auto-correlations of the NAO index are presented. Based on the results presented in the current study, a long-term oscillation with a 70 to 80 year cycle may exist in the Pacific and Atlantic regions simultaneously. Because the slow and cyclic long-term oscillation can be predictable using EMD, if the same climate conditions of the Pacific and Atlantic Oceans continue as the last several decades, the spatial evolution of climate variables might also be inferred according to the phase of the long-term oscillation. Further physical study and analysis of long proxy records should help provide more conclusive results. Copyright © 2012 Royal Meteorological Society

KEY WORDS empirical mode decomposition; Pacific Decadal Oscillation; North Atlantic Oscillation; long-term oscillation

Received 8 September 2011; Revised 30 January 2012; Accepted 10 March 2012

1. Introduction and methodology

Climatic variations in the Pacific and Atlantic Oceans are critical for the modelling and the prediction of global climate. Atmospheric teleconnections point out to the communication between the two Oceans. This is referred to as the atmospheric bridge, called teleconnections (Wallace and Gutzler, 1981; Klein *et al*., 1999; Rogers and Coleman, 2003). A number of publications presented evidence that these two regions are teleconnected to each other (Enfield and Mayer, 1997; Vecchi and Soden, 2007). The climate conditions of these two regions are described with a number of climate indices. Among these indices, the Pacific Decadal Oscillation (PDO) index (Mantua *et al*., 1997) and the North Atlantic Oscillation (NAO) index (Visbeck *et al*., 2001) are commonly accepted to reflect the major climate conditions of the Pacific and Atlantic Oceans.

* Correspondence to: T. Lee, 501 Jinju-daero, Jinju, Gyeongsangnam-do 660–701, South Korea. E-mail: tae3lee@gnu.ac.kr

In this study, we investigated the interconnection between the Pacific and Atlantic Oceans using these two representative climate indices using a spectral analysis. Until now, most of studies on spectral analysis of NAO and PDO focused on either finding abrupt changes (Schwing *et al*., 2003) or identifying a range of significant frequencies during a certain time period using frequency analyses and assuming an *a priori* basis (e.g. a mother wavelet in wavelet analysis) (Torrence and Compo, 1998; Labat *et al*., 2004). However, in the current study an empirical frequency technique, called empirical mode decomposition (EMD) (Huang and Wu, 2008; Lee and Ouarda, 2010) was used to analyse the NAO and PDO indices.

The empirical signals and connections hidden in the NAO and PDO indices are shown through the EMD components for different frequency levels. The variations and the correlation structures of high-frequency components according to the phase of the low-frequency components are investigated. Furthermore, global spatial patterns of climate variables are also analysed during the long-term warm and cold periods identified from the low-frequency EMD components of two indices.

2. Methods and data

2.1. Empirical mode decomposition

To investigate the association of long-term oscillations as well as short-term modes between NAO and PDO indices, EMD analysis was applied (Huang *et al.*, 1998; Huang and Wu, 2008). EMD is an algorithm that extracts nonstationary oscillation components into the intrinsic mode functions (IMFs) from a targeted time series in order to yield physically meaningful explanations of the time series. To find significant components, a significance test (Wu and Huang, 2004) was developed. This test was used to compare the relationship of the mean period and the mean normalized energy of the IMFs of the target time series with the IMFs from normal random independent sequences. Unlike other time frequency analyses (e.g. wavelet analysis), the EMD procedure directly decomposes the original signal into a finite number of components (Lee and Ouarda, 2010, 2011, 2012).

The procedure to obtain IMFs from a time series, X, is as follows: (1) identify all of the local extrema and connect all local maxima (minima) with a cubic spline as the upper (lower) envelope; (2) obtain the first component (h) by finding the difference between the data and the local mean of the upper and lower envelopes (m) as $h = X - m$; (3) substitute X by h and repeat steps (1) and (2) until a certain criterion in which the component (h) is guaranteed to retain enough physical sense of both amplitude and frequency modulations (Huang *et al.*, 1998) is met; (4) designate the final h as the jth IMF, c_j, and the residue is r_j (i.e. $r_j = r_{j-1} - c_j$ where $r_0 = X$); and (5) repeat steps (1)–(4) by treating the residue r_j as the original data until the final residue becomes a monotonic function. The final residue (r_n) becomes c_{n+1}. Then the original time series, X, is presented as the sum of the estimated IMFs as

$$X = \sum_{j=1}^{n+1} c_j \tag{1}$$

Note that lower order components have a higher frequency level and vice versa. For example, the highest frequency level component is c_1.

2.2. Data description

NAO is a large seesaw in atmospheric mass between the Icelandic low and the Azores high (Visbeck *et al.*, 2001). A zonal-average version was introduced by Li and Wang (2003a, 2003b) and used in the current study instead of the instrumental record-based indices (Cullen *et al.*, 2002). The NAO index ($\mathrm{NAO_{LW}}$) is denoted as

$$\mathrm{NAO_{LW}} = P^*_{35\mathrm{N}} - P^*_{65\mathrm{N}} \tag{2}$$

where P^*_θ is the standardized monthly sea-level pressure (SLP) anomalies over the longitude of 80 °W–30 °E at the latitude of θ. The yearly NAO index was formed by averaging the monthly NAO index.

The PDO index represents the leading principal component of sea-surface temperature (SST) anomalies in the North Pacific Ocean, polewards of 20 °N. Among a number of PDO indices, the most commonly used one developed by Mantua *et al.* (1997) was used.

In the current study, SLP (Pa), precipitable water (PW; kg m^2), and SST (Kelvin) are selected to determine the global climate effects along with the long-term oscillations of the two indices. The global SLP and PW data were acquired from the dataset of the National Centers for Environmental Prediction and the National Center for Atmospheric Research (NCEP/NCAR) reanalysis data (Kalnay *et al.*, 1996), for the period 1948–2008. National Oceanic and Atmospheric Administration (NOAA) extended, reconstructed data were used for SST for the period 1900–2008 (Smith *et al.*, 2007). Yearly anomalies were estimated from the monthly dataset by subtracting the monthly mean relative to years 1961–1990 and averaging the monthly anomalies for each year.

3. Results

3.1. EMD analysis on the NAO and PDO indices

An EMD analysis indicated the presence of a considerable interconnection between the two indices in both long-term and short-term frequencies, as shown in Figure 1. The average of the two summed critical long-term oscillations (4th and 5th components) from the EMD analysis and its significance test (Wu and Huang, 2004, 2005) as well as the time series of the NAO and PDO indices are presented in Figure 1(a). Moreover, the most significant long-term oscillation component (the 5th) from the significance test (Wu and Huang, 2004), with around a 70 to 80 year cycle, shows that this long-term oscillation pattern exists in both signals (Figure 1(b)). The magnitudes and cycles for the long-term oscillation component of both signals match well. The slight deviation between the two 5th components (i.e. the PDO's 5th component is slightly shorter than the NAO's, Figure 1(b)) is inevitable because random noise processes and other components might slightly perturb the 5th oscillation process during the EMD analysis (Huang *et al.*, 1998; Huang and Wu, 2008). There could be an internal (Haines, 1994) or external (McGuffie and Henderson-Seller, 2005) driving force or a combination of both (Latif *et al.*, 2009) that induces this long-term oscillation simultaneously in the Pacific and Atlantic Oceans. In short, Figures 1(a) and (b) reveal that the two indices share the same long-term oscillation (a 70 to 80 year cycle).

Furthermore, the magnitude of the cross-correlation between the two indices and the serial correlation of each index vary according to the phase of the long-term oscillation, especially over the last 60 years (see

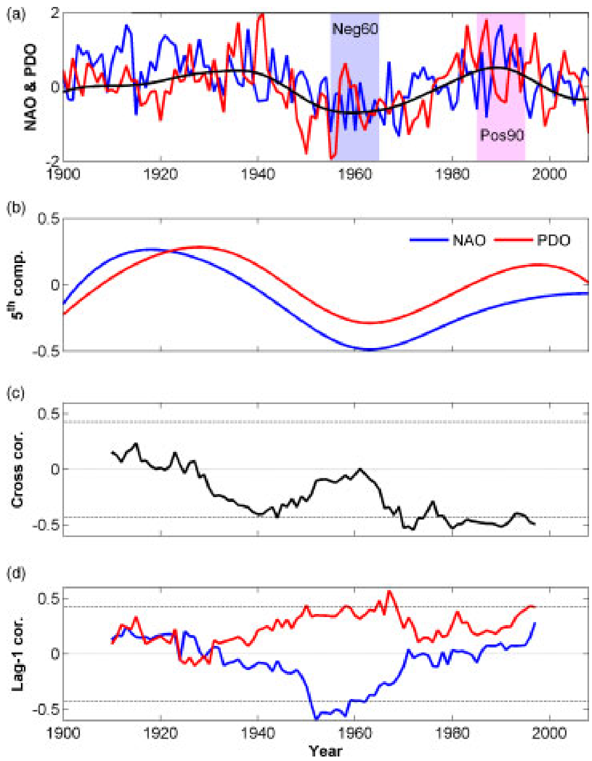

Figure 1. (a) Time series of the North Atlantic Oscillation (NAO) (blue) and Pacific Decadal Oscillation (PDO) (red) indices and the average of the 4th + 5th components from empirical mode decomposition (EMD) for NAO and PDO (black); (b) 5th component of both indices of the NAO and PDO indices; (c) the cross-correlation of the remaining components (the original time series minus the 4th + 5th components) with a 21 year moving window (10 years before and 10 years after the centre) and the bounds as ±1.96/sqrt(n) (Brockwell and Davis, 2003) with $n = 21$ (dashed line); and (d) lag-1 serial correlation of the remaining components of a 21 year moving window for the NAO and PDO indices with the bounds. This figure is available in colour online at wileyonlinelibrary.com/journal/joc

Figures 1(c) and (d)). As shown in Figure 1(c), the cross-correlations between the residuals of the NAO and PDO indices with a 21 year window (10 years before to 10 years after the centre) are significantly negative after 1970 to the present, while around 1950–1970 no significant cross-correlation is observed. The lag-1 serial-correlation of the residuals (the original data minus the 4th and 5th components) shown in Figure 1(d) is negative for the NAO index and positive for the PDO index during 1955–1965, while outside this period, not much significant correlation is observed.

In order to draw the spatial implications of the observed long-term variations shown in Figure 1, the spatial patterns of the global climate variables as well as their correlation structures are analysed in the following three sections.

3.2. Global climate variation and long-term oscillation of climate indices

The long-term oscillation presents a negative phase centered on the year 1960 (Neg60, years 1955–1965) and a positive phase centered on the year 1990 (Pos90, years 1985–1995). The spatial patterns of the selected climate variables (i.e. SLP, PW, and SST) over these two periods (Neg60 and Pos90) are displayed in order to reveal the existence and the global effect of the long-term oscillation (refer to Figure 2).

The mean yearly anomalies of the SLP for Neg60 and Pos90 are displayed in Figure 2(a-1) and (a-2). In these figures, blue regions indicate values lower than the mean of 1961–1990, whereas red regions indicate higher values. Notably low SLP is then observed over North Africa and the middle of Asia, which represent arid climate zones in Figure 2(a-1). The lower-than-normal pressure over the arid zone is related to the precipitation, because rainy days are more likely in a lower-pressure condition than at higher pressure. A considerably high positive quantity of PW over North Africa is observed in Figure 2(b-1) as expected.

On the contrary, Figure 2(a-2) shows that the mean yearly anomalies of the SLP during the Pos90 are the opposite of the anomalies of the Neg60, such that a lower SLP over both poles and a slightly higher SLP over North Africa and the middle of Asia were present during the Pos90. The higher SLP over North Africa might be expected to lower the precipitation of this region, as shown in Figure 2(b-2), in opposition to the years 1955–1965. In Figures 2(c-1) and (c-2), the mean yearly anomalies of the SST over the Neg60 and the Pos90 show opposite spatial patterns over various regions. The positive-anomaly regions during the Neg60, such as the North Atlantic near Greenland and the middle Pacific, present negative values during the Pos90. Notice that, in the region between 35 °N and 65 °N, the Pacific and Atlantic Oceans show opposite tendencies during the Pos90 period (35 °N, cold Pacific and warm Atlantic; 65 °N, warm Pacific, cold Atlantic) shown in Figure 2(c-2), while this spatial tendency is not obvious during the Neg60 (Figure 2(c-1)). The negative-anomaly regions, especially the Southern Hemisphere during the Neg60, show a slightly positive anomaly during the Pos90. The overall spatial tendency of SST is summarized in Figure 2(c-3).

The difference maps of the mean yearly anomalies between the Pos90 and the Neg60 (the anomalies of the Pos90 minus the ones of the Neg60) for SLP, PW, and SST are illustrated in Figures 2(a-3), (b-3) and (c-3), respectively. The red regions indicate an increase of a variable during the Pos90 period compared to the Neg60, while the blue regions indicate a decrease in the variable. As shown in Figure 2(a-3), the Pos90 SLP is higher than the Neg60 in Africa and Eurasia. In particular, the desertic regions (North Africa and the middle of Asia) and southern Europe show a relatively significant increase. For the NAO index (the difference of the SLP 35 °N and the SLP 65 °N, Equation (2)), it is obvious that the decrease of the SLP over the Azores High (blue) region and the increase of the Icelandic Low (red) region led to the variation of the NAO index from the negative phase over the Neg60 period to the positive phase over the Pos90 period.

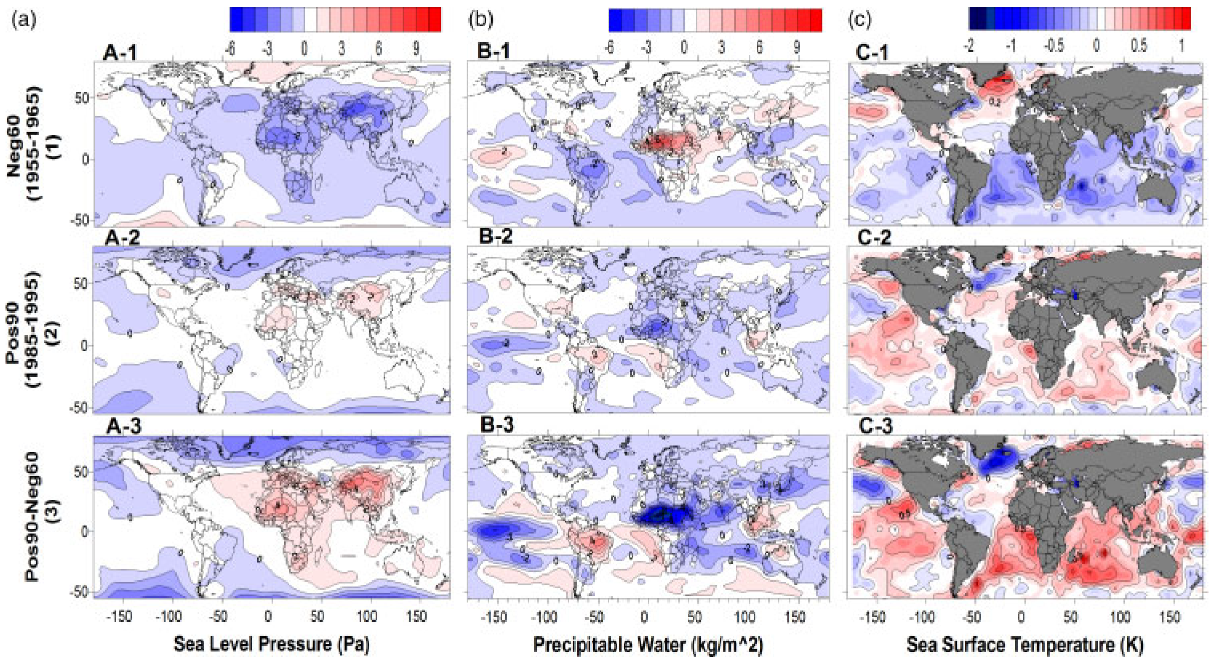

Figure 2. Mean yearly anomalies (MYA) of three variables relative to 1961–1990 such as (a) sea-level pressure (SLP), (b) precipitable water (PW), and (c) sea-surface temperature (SST) of years (1) Neg60 (1955–1965), (2) Pos90 (1985–1995), and (3) difference map of MYA between Pos90 and Neg60. Positive values are in red color and negative values in blue color. Each contour line presents 1 Pa (SLP), 1 kg m^2 (PW), and 0.2 K (SST) difference. *X* and *Y* coordinates present the longitude and latitude (degree) for each plot. This figure is available in colour online at wileyonlinelibrary.com/journal/joc

The spatial pattern of precipitable water might be expected to follow the conditions of the SLP shown in Figure 2(b-3). The most significant difference is observed around the North African (Sahara desert) region. The high negative values (dark-blue region) indicate the significant reduction in precipitation related to the desertification of this region. The region where the significant precipitation reduction occurred includes the watershed of the Niger River. The time series of the Niger River at Koulikoro, which covers the western part of the Niger River basin, is shown in Figure 3. It reveals that a much higher volume of stream flow was observed during the Neg60 than during the Pos90 period. This coincides with the results shown in Figures 2(b-1), (b-2) and (b-3). In contrast, the Amazon region shows an increase in precipitable water along with South Australia. The magnitude is not very significant compared to the Niger River basin.

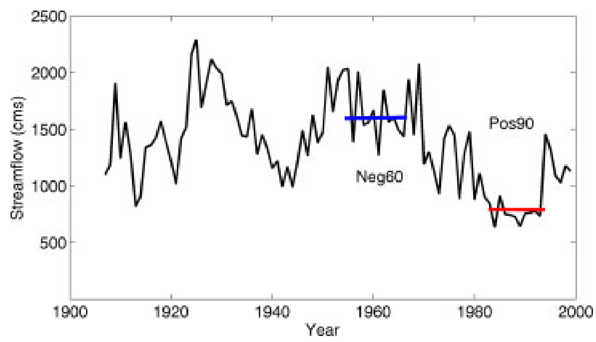

Figure 3. Time series at Koulikoro station in cubic meter per second (CMS). Notice that the area covered by the flow of Koulikoro station is the west side of the Niger River basin. Details can be found in the website http://www.crwr.utexas.edu/gis/gishyd98/atlas/ESRI97/Esri.htm. This figure is available in colour online at wileyonlinelibrary.com/journal/joc

3.3. Cross-correlation study between climate indices and global gridded variables

Further investigation of the long-term variation of the cross-correlations between the residuals of the NAO and PDO indices, as shown in Figure 1(c), was carried out in this section. The cross-correlations between the PDO index and the global SLP over the extended Neg60 (1950–1970) and the extended Pos90 (1980–2000) periods were estimated, and the results are presented in Figures 4(a) and (b), respectively. During the extended Neg60 period, the PDO index was negatively correlated with the whole Pacific region and the middle and north Atlantic, while it was positively correlated with the eastern side of Greenland and the south Atlantic (Figure 4(a)). Notice that the negative cross-correlation of the North Atlantic Ocean near 35 °N was stronger during the extended Pos90 (Figure 4(b)). At the same time, a positive cross-correlation with the PDO index is observed above 65 °N of this region during this period. Therefore, these spatial patterns lead to the conclusion that the negative correlation between the PDO and NAO indices for the extended Pos90 (see Figure 1(c)) was influenced by the negative correlation of PDO with the 35 °N region and the positive correlation of PDO with the 65 °N region. The proof of this cross-correlation structure is provided in Equation (A4) of Appendix A. for the case of the NAO index (NAO_{LW} in Equation (2)).

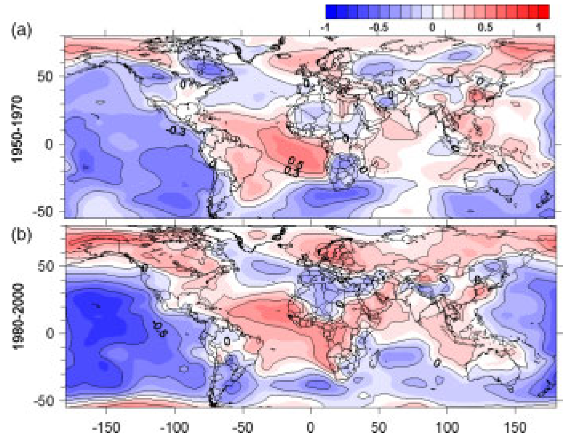

Figure 4. Cross-correlation between Pacific Decadal Oscillation and sea-level pressure yearly anomalies for years (a) 1950–1970 and (b) 1980–2000. Each contour line presents 0.2 difference. This figure is available in colour online at wileyonlinelibrary.com/journal/joc

3.4. Serial correlation study of global gridded variables related to climate indices

The long-term variation of the lag-1 correlation estimated from the residuals of the PDO and NAO indices shown in Figure 1(d) was further analysed for the global climate variables (i.e. SLP and SST). The lag-1 correlation of the global SLP and SST was estimated for the extended Neg60 and the extended Pos90 periods and is presented in Figure 5. During the extended Neg60 (Figure 5(a-1)), the SLP had a stronger temporal self-dependent structure globally than during the extended Pos90 (Figure 5(a-2)). During the extended Neg60, a strong positive serial correlation is observed in Africa, South America, and middle Asia, whereas a significant negative serial correlation is seen in Greenland and nearby northern Europe. The strong negative SLP lag-1 serial correlation in the mid-Atlantic (35°N) and Greenland (65°N) described in Figure 5(a-1) for the extended Neg60 (blue line of Figure 1(d)) might drive the negative serial correlation in the NAO index during the same period (refer to Equation (A7) of Appendix A). No significant persistence over the SST can be observed (Figure 5(b-1) and (b-2).

4. Remarks and conclusions

The results of the current study reveal that (1) the representative climate indices of the Pacific and Atlantic Oceans, PDO and NAO, share the same long-term oscillation pattern over the Neg60 and Pos90 periods; and (2) according to the phase condition of the long-term oscillation, the cross-correlation between the two indices and the autocorrelation structure of each index varies in strength for the extended Neg60 and the extended Pos90. The global climate condition over the negative and positive periods shows a particular spatial tendency in SLP, PW, and SST. The burgeoning negative period starting from around year 2005 is also analysed. Somewhat similar spatial tendency to Neg60 is observed in SLP, PW, and SST variables even though it is not clear because of the short available record (data not shown).

Overall, a long-term oscillation with a 70 to 80 year cycle may exist in the Pacific and Atlantic regions, and global climate variables follow the conditions of the long-term cycle. This long-term cycle is also discussed by Keenlyside *et al*. (2008) for the North Atlantic sector. If the long-term oscillation continues to vary smoothly and cyclically similarly to the last several decades presented in the current study, the spatial evolution of climate variables might be predictable with a time-series simulation technique (Smith *et al*., 2007; Lee and Ouarda, 2010). However, the number of long-term cycles is still too limited to lead the firm conclusion. Further physical study and the analysis of long proxy records of climate indices (Shen *et al*., 2006) might be useful to confirm the long-term oscillation because the current time series of the two climate indices contain only one full 70 to 80 year cycle.

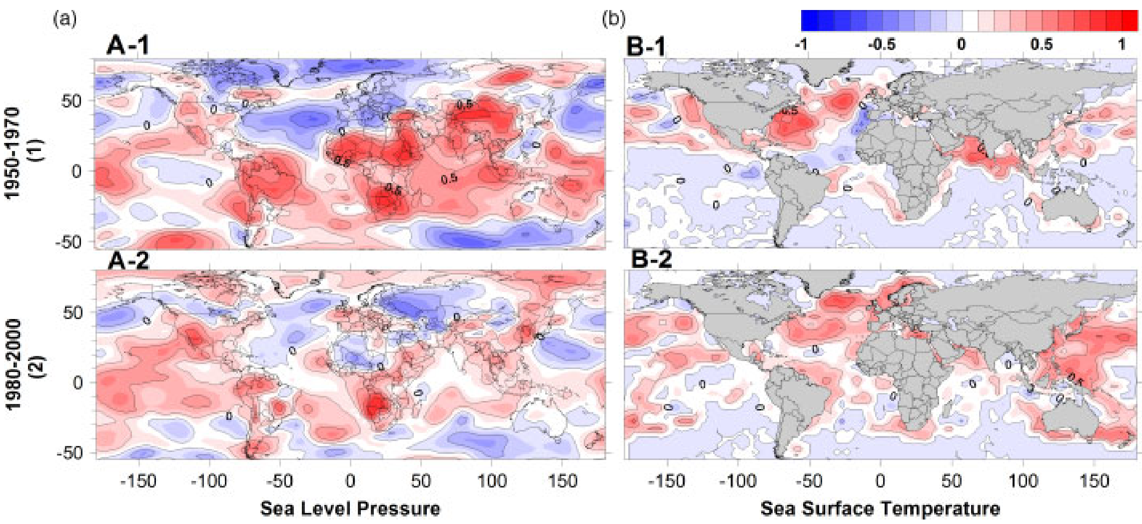

Figure 5. Lag-1 serial correlation of (a) sea level pressure and (b) sea surface temperature yearly anomalies for years (1) 1950–1970 and (2) 1980–2000. Each contour line presents 0.2 difference. This figure is available in colour online at wileyonlinelibrary.com/journal/joc

Appendix A. Lag-1 serial correlation of NAO and cross-correlation between NAO and PDO

Assume that Z_t represents the NAO index introduced in the original manuscript with time index t and that X_t and Y_t are the scaled SLP over the Atlantic region for 35 °N and 65 °N, respectively (Li and Wang, 2003). Therefore, the NAO (Z_t) is represented as

$$Z_t = X_t - Y_t \tag{A1}$$

Assume that A_t is another variable indicating the PDO index,

$$A_t Z_t = A_t X_t - A_t Y_t \tag{A2}$$

The expectation is

$$E[A_t Z_t] = E[A_t X_t] - E[A_t Y_t] \tag{A3}$$

With zero mean for all the variables, the covariance is

$$\text{cov}(AZ) = \text{cov}(AX) - \text{cov}(AY) \tag{A4}$$

If $\text{cov}(AX) < 0$ and $\text{cov}(AY) > 0$, then it follows that $\text{cov}(AZ) < 0$.

As the variance is generally always greater than zero, this implies that, if A and X are negatively correlated and A and Y are positively correlated, then A and Z are negatively correlated.

For lag-1 serial correlation,

$$Z_{t-1} Z_t = X_t (X_{t-1} - Y_{t-1}) - Y_t (X_{t-1} - Y_{t-1}) \tag{A5}$$

Without loss of generality, $E(X_t Y_{t-1}) = E(Y_t X_{t-1}) = 0$; then

$$E[Z_t Z_{t-1}] = E[X_t X_{t-1}] + E[Y_t Y_{t-1}] \tag{A6}$$

With zero mean for all the variables,

$$\text{cov}(Z_t Z_{t-1}) = \text{cov}(X_t X_{t-1}) + \text{cov}(Y_t Y_{t-1}) \tag{A7}$$

If $\text{cov}(X_t X_{t-1}) < 0$ and $\text{cov}(Y_t Y_{t-1}) < 0$, then surely $\text{cov}(Z_t Z_{t-1}) < 0$.

As the variance is generally always greater than zero, this implies that, if X_t and X_{t-1} are negatively correlated and Y_t and Y_{t-1} are negatively correlated, then Z_t and Z_{t-1} are negatively correlated as well.

References

Brockwell PJ, Davis RA. 2003. *Introduction to Time Series and Forecasting*. Springer: Harrisonburg.

Cullen HM, Kaplan A, Arkin PA, Demenocal PB. 2002. Impact of the North Atlantic Oscillation on Middle Eastern climate and streamflow. *Climatic Change* **55**: 315–338.

Enfield DB, Mayer DA. 1997. Tropical Atlantic sea surface temperature variability and its relation to El Nino Southern Oscillation. *Journal of Geophysical Research-Oceans* **102**: 929–945.

Haines K. 1994. Low-frequency variability in atmospheric middle latitudes. *Surveys in Geophysics* **15**: 1–61.

Huang NE, Shen Z, Long SR, Wu MLC, Shih HH, Zheng QN, Yen NC, Tung CC, Liu HH. 1998. The empirical mode decomposition and the Hilbert spectrum for nonlinear and non-stationary time series analysis. *Proceedings of the Royal Society of London Series a-Mathematical Physical and Engineering Sciences* **454**: 903–995.

Huang NE, Wu ZH. 2008. A review on Hilbert-Huang transform: method and its applications to geophysical studies. *Reviews of Geophysics* **46**: RG2006, 23pp.

Kalnay E, Kanamitsu M, Kistler R, Collins W, Deaven D, Gandin L, Iredell M, Saha S, White G, Woollen J, Zhu Y, Chelliah M, Ebisuzaki W, Higgins W, Janowiak J, Mo KC, Ropelewski C, Wang J, Leetmaa A, Reynolds R, Jenne R, Joseph D. 1996. The NCEP/NCAR 40 year reanalysis project. *Bulletin of the American Meteorological Society* **77**: 437–471.

Keenlyside NS, Latif M, Jungclaus J, Kornblueh L, Roeckner E. 2008. Advancing decadal-scale climate prediction in the North Atlantic sector. *Nature* **453**: 84–88.

Klein SA, Soden BJ, Lau NC. 1999. Remote sea surface temperature variations during ENSO: evidence for a tropical atmospheric bridge. *Journal of Climate* **12**: 917–932.

Labat D, Ronchail J, Callede J, Guyot JL, De Oliveira E, Guimaraes W. 2004. Wavelet analysis of Amazon hydrological regime variability. *Geophysical Research Letters* **31**.

Latif M, Park W, Ding H, Keenlyside NS. 2009. Internal and external North Atlantic sector variability in the Kiel climate model. *Meteorologische Zeitschrift* **18**: 433–443.

Lee T, Ouarda TBMJ. 2010. Long-term prediction of precipitation and hydrologic extremes with nonstationary oscillation processes. *Journal of Geophysical Research-Atmospheres* **115**: D13107, DOI:10.1029/2009JD012801.

Lee T, Ouarda TBMJ. 2011. Prediction of climate nonstationary oscillation processes with empirical mode decomposition. *Journal of Geophysical Research-Atmospheres* **116**: D13107, DOI: 10.1029/2010JD015142.

Lee T, Ouarda TBMJ. 2012. Stochastic simulation of nonstationary oscillation hydro-climatic processes using empirical mode decomposition. *Water Resources Research*. **48**: W02514, 15pp.

Li JP, Wang JLXL. 2003a. A modified zonal index and its physical sense. *Geophysical Research Letters* **30**: 34.1–34.4.

Li JP, Wang JLXL. 2003b. A new North Atlantic Oscillation index and its variability. *Advances in Atmospheric Sciences* **20**: 661–676.

Mantua NJ, Hare SR, Zhang Y, Wallace JM, Francis RC. 1997. A Pacific interdecadal climate oscillation with impacts on salmon production. *Bulletin of the American Meteorological Society* **78**: 1069–1079.

McGuffie K, Henderson-Seller A. 2005. *A Climate Modelling Primer*. Wiley: Chichester, 23–26.

Rogers JC, Coleman JSM. 2003. Interactions between the Atlantic Multidecadal Oscillation, El Nino/La Nina, and the PNA in winter Mississippi valley stream flow. *Geophysical Research Letters* **30**: D06107, 15pp.

Schwing FB, Jiang JM, Mendelssohn R. 2003. Coherency of multi-scale abrupt changes between the NAO, NPI, and PDO. *Geophysical Research Letters* **30**: 1406, 4pp.

Shen CM, Wang WC, Gong W, Hao ZX. 2006. A Pacific Decadal Oscillation record since 1470 AD reconstructed from proxy data of summer rainfall over eastern China. *Geophysical Research Letters* **33**: L03702, 4pp.

Smith DM, Cusack S, Colman AW, Folland CK, Harris GR, Murphy JM. 2007. Improved surface temperature prediction for the coming decade from a global climate model. *Science* **317**: 796–799.

Torrence C, Compo GP. 1998. A practical guide to wavelet analysis. *Bulletin of the American Meteorological Society* **79**: 61–78.

Vecchi GA, Soden BJ. 2007. Increased tropical Atlantic wind shear in model projections of global warming. *Geophysical Research Letters* **34**: L08702, 5pp.

Visbeck MH, Hurrell JW, Polvani L, Cullen HM. 2001. The North Atlantic Oscillation: Past, present, and future. *Proceedings of the National Academy of Sciences of the United States of America* **98**(23): 12876–12877.

Wallace JM, Gutzler DS. 1981. Teleconnections in the geopotential height field during the Northern Hemisphere winter. *Monthly Weather Review* **109**: 784–812.

Wu ZH, Huang NE. 2004. A study of the characteristics of white noise using the empirical mode decomposition method. *Proceedings of the Royal Society of London Series a-Mathematical Physical and Engineering Sciences* **460**: 1597–1611.

Wu ZH, Huang NE. 2005. In *Hilbert-Huang Transform and Its Applications*, Huang NE, Shen SP (eds). World Scientific Publishing Company: Hackensack, NJ, 125–148.

